metals

MDPI

Article

Effect of Interval Time Between Pre-Deformation and Artificial Aging on Mechanical Properties of Er-Containing 7075 Aluminum Alloy

Yingze Liu [1,*], Zhiqian Liao [1,2], Desheng Wang [1,2,*], Guoyuan Liu [1], Jiangyi Ren [1], Wenfu Li [1], Yunao Yang [1], Lingjie Chen [1] and Yue Wang [2]

[1] Luoyang Ship Material Research Institute, Binhe South Road, Luoyang 471000, China
[2] National Key Laboratory of Marine Corrosion and Protection, Luoyang Ship Material Research Institute, Luoyang 471023, China
* Correspondence: liuyingze@725.com.cn (Y.L.); wangdesheng07@163.com (D.W.); Tel.: +86-132-2821-0273 (Y.L.)

Abstract

In order to obtain the optimal heat treatment process of Er-containing 7075 aluminum alloy, the effects of pre-stretching and the interval time between pre-stretching and aging on the microstructure and mechanical properties of Er-containing 7075 aluminum alloy during solution treatment followed by pre-stretching and two-stage aging processes were investigated by mechanical property tests, metallographic tests, scanning electron microscopy (SEM), and transmission electron microscopy (TEM). The results show that the mechanical properties of Er-containing 7075 aluminum alloy can be significantly improved by increasing the extrusion ratio. Pre-stretching provides nucleation sites for the precipitation of reinforcing phases, accelerates the aging strengthening process, and shortens the peak aging time. The crack source of fracture in Er-containing 7075 aluminum alloy is attributed to the segregated second phases containing Cu and Er in the alloy. The research results have significant engineering significance for the optimization of the heat treatment process of Er-containing 7075 aluminum alloy.

Keywords: wrought Er-containing 7075 aluminum alloy; heat treatment; pre-stretch; double step aging

check for updates

Academic Editor: Sebastian Feliú, Jr.

Received: 9 May 2025
Revised: 1 July 2025
Accepted: 14 July 2025
Published: 28 July 2025

Citation: Liu, Y.; Liao, Z.; Wang, D.; Liu, G.; Ren, J.; Li, W.; Yang, Y.; Chen, L.; Wang, Y. Effect of Interval Time Between Pre-Deformation and Artificial Aging on Mechanical Properties of Er-Containing 7075 Aluminum Alloy. *Metals* **2025**, *15*, 841. https://doi.org/10.3390/met15080841

Copyright: © 2025 by the authors. Licensee MDPI, Basel, Switzerland. This article is an open access article distributed under the terms and conditions of the Creative Commons Attribution (CC BY) license (https://creativecommons.org/licenses/by/4.0/).

1. Introduction

Adding rare earth elements to 7075 aluminum alloy can improve the overall properties of the alloy; for example, adding Er elements to 7075 aluminum alloy can improve the strength and corrosion resistance of 7075 aluminum alloy [1,2]. The yield strength and tensile strength of er-containing 7075 aluminum alloy in a T73 heat treatment state are 30 MPa and 50 MPa higher than that of 7075 aluminum alloy, respectively, and have similar elongation. And Er-containing 7075 aluminum alloy has better stress corrosion resistance and seawater corrosion resistance, and is widely used in the shipbuilding industry [3–5].

Similarly to the Al-Zn-Mg-Cu aluminum alloy in the 7xxx series, Er-containing 7075 aluminum alloy is a heat-treatment-hardening alloy, and the heat treatment process is generally a solid-solution artificial-aging process [6]. Solid solution quenching is used to make alloy elements fully soluble into an aluminum matrix to form a supersaturated solid solution. The natural aging speed of Al-Zn-Mg-Cu aluminum alloys is slow, and it is difficult to reach a stable state even if the natural aging is several years, so artificial aging is generally used [7–10]. Being kept at room temperature after solution quenching

before artificial aging has a certain effect on the properties of alloys, and this effect is most harmful when the residence time is 4~30 h [11]. This is related to the regression of the GP zone produced by the aluminum alloy staying at room temperature.

In order to eliminate the harm of being at room temperature, a two-stage artificial aging process can be used [12–14]. Two-stage aging is a process that can obtain an over-aging effect in a shorter aging time. At a lower first-stage aging temperature, a relatively stable GP zone can be formed, and then at a higher second-stage aging temperature, it becomes the core of "phase precipitation, making it disperse and distribute uniformly [15,16]. In addition to the conventional solution and artificial aging treatment, deformation heat treatment is also an effective means to strengthen aluminum alloys. Through plastic deformation, the density of defects (mainly dislocations) in metals can be increased, and the distribution of various crystal defects can be changed [17]. If the alloy undergoes phase transformation during or after deformation, the change in defect configuration and defect density during deformation has a great influence on the nucleation kinetics and the distribution of new phases [18–20]. On the contrary, the formation of new phases often pins and hinders the movement of defects such as dislocations, so as to stabilize the defects in metals. Cold deformation after quenching, on the one hand, can eliminate the residual stress introduced by solution quenching; on the other hand, it can also increase the defect density in the aluminum alloy, provide more nucleating particles for aging precipitates, and accelerate precipitation strengthening [21]. Li et al. [22] demonstrated that 0.15–0.25% Er reduced secondary dendrite arm spacing by 40% without forming Al_3Zr. It should be noted that Al_8Cu_4Er consumes Cu, altering T-phase composition. Wu et al. [23] established dual-stage homogenization (400 °C/10h + 465 °C/24h), which enables complete $Al_3(Er,Zr)$ precipitation while eliminating 92% of eutectic phases. Yuan et al. [24] reported an optimal value of 0.2% Er reduces DAS_1 by 28% and DAS_2 by 33% in directionally solidified alloys. Excess Er (>0.3%) causes brittle Al_8Cu_4Er network formation.

In order to prepare low-stress aluminum alloy tubes with a stable phase state and to correct the shape of hot extruded tubes, pre-stretching deformation technology is often introduced after solid solution quenching of extruded tubes [25–28]. Pre-denaturation will introduce defects such as vacancy defects, dislocation line defects, and interface defects into the aluminum alloy structure. These defects can be used as nucleation particles for the desolubilization of alloy elements in the aging process, and accelerate the aging process. The study of pre-deformation technology is introduced by citing the literature. However, at present, the research on pre-deformation heat treatment technology of aluminum alloys lacks consideration of the interval time between pre-deformation and aging on the microstructure and mechanical properties of aluminum alloys [29]. At the same time, research results on the corrosion properties of Er-containing 7075 aluminum alloy after solution, pre-tensile and aging treatment are also lacking.

In this paper, a new heat treatment method was proposed for Er-containing 7075 aluminum alloy, where the extruded aluminum alloy tubes are quenched by solution, cold deformation and tensile treatment, and are then subjected to double-stage aging. The mechanical properties of aluminum alloys were tested at different intervals. The effect of interval time between pre-deformation and artificial aging on mechanical properties was investigated for the first time. The mechanical properties of the two-stage aging treatment and two-stage aging treatment after pre-stretching were compared, and the effect of pre-stretching on the mechanical properties of Er-containing 7075 aluminum alloy were illustrated by setting up a natural aging group. The corrosion behavior of Er-containing 7075 aluminum alloy treated by solution, pre-tensile treatment and two-stage aging was studied.

2. Materials and Methods

2.1. The Starting Materials

The experimental material used in the study was the Er-containing 7075 seamless extruded tube purchased from Northwest Aluminum Co., Ltd. (Lanzhou, China). The ingots were cast by semi-continuous casting. The ingots were then extruded into seamless tubes on a horizontal extruder with different extrusion die/extrusion ratios. The chemical content range of the Er-containing 7075 aluminum alloy is shown in Table 1. The raw extrusion tubes have two different extrusion ratios; the extrusion ratios were 8 and 12, respectively.

Table 1. Chemical composition of Er-containing 7075 aluminum alloy (wt.%).

Element	Zn	Mg	Cu	Mn	Zr	Er	Fe	Si	Al
Content range	5.5~6.6	1.8~2.6	1.0~1.6	0.08~0.12	0.06~0.12	0.08~0.12	≤0.15	≤0.10	Balanced

2.2. Heat Treatment

The heat treatment experiment scheme is shown in Table 2. The furnace temperature uniformity of the heat treatment furnace equipment used is ±3 °C. And the schematic diagram of the heat treatment process is shown in Figure 1. The extrusion ratio of Group A materials was 12, and that of Group B, C and D materials was 8. Group A1 and B1 refer to extruded tubing that has undergone solution treatment and pre-stretching, followed by natural aging for 180 days. Group A2 and Group B6 refer to extruded tubing that has undergone solution treatment and pre-stretching, followed by natural aging for 180 days, and subsequently undergoing a two-step artificial aging treatment. Groups B2 to B5 refer to tubing that has undergone solution treatment and pre-stretching, and which were then left for 24 h, 15 days, and 30 days, respectively, before undergoing a two-step aging treatment. Groups C1 to C8 refer to tubing that has undergone solution treatment without pre-stretching, and which were then subjected to two-step artificial aging treatments for different durations. Groups D1 to D6 refer to tubing that has undergone solution treatment, followed by natural aging for 0.5 h, 2 h, 4 h, 8 h, 24 h, and 48 h, respectively.

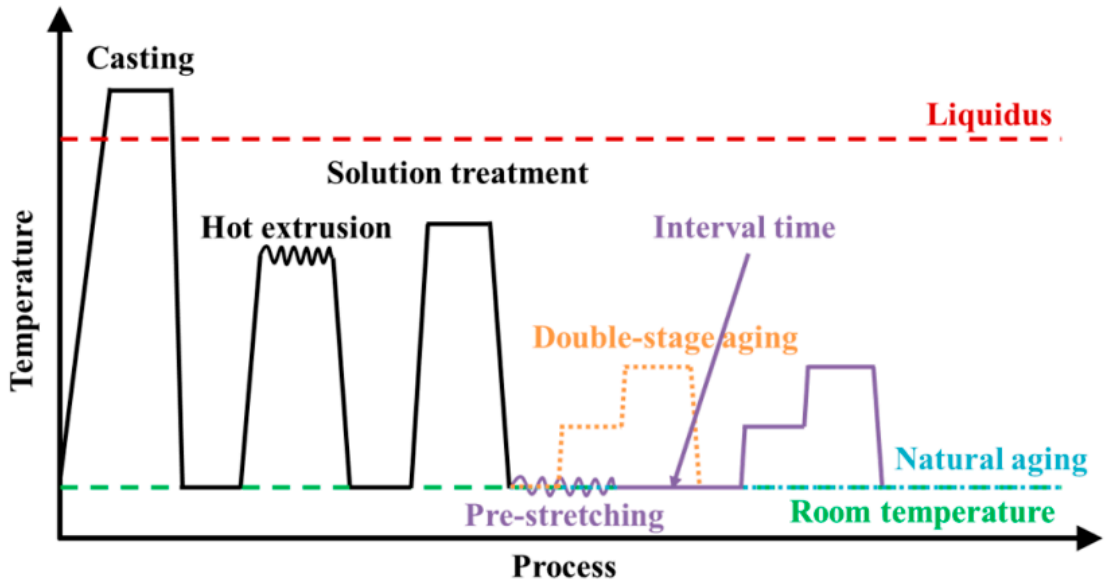


Figure 1. A schematic diagram of the heat treatment process.

Table 2. Experimental parameters of Er-containing 7075 aluminum alloy heat treatment.

Number	Solution Treatment	Pre-Tensile	Interval Time	Aging Treatment
A1	470 °C × 1 h + 500 °C × 2 h	2.0%	None	Natural aging 180 d
A2			/	Natural aging 180 d + 110 °C × 5 h + 150 °C × 12 h
B1			None	Natural aging 180 d
B2			24 h	110 °C × 5 h + 150 °C × 12 h
B3			15 d	
B4			30 d	
B5			/	None
B6		None	/	Natural aging 180 d + 110 °C × 5 h + 150 °C × 12 h
C1		None	None	110 °C × 3 h
C2		None	None	110 °C × 5 h
C3		None	None	120 °C × 5 h + 163 × 3 h
C4		None	None	120 °C × 5 h + 163 × 6 h
C5		None	None	120 °C × 5 h + 163 × 9 h
C6		None	None	120 °C × 5 h + 163 × 12 h
C7		None	None	120 °C × 5 h + 163 × 15 h
C8		None	None	120 °C × 5 h + 163 × 18 h
D1		None	None	Natural aging 0.5 h
D2		None	None	Natural aging 2 h
D3		None	None	Natural aging 4 h
D4		None	None	Natural aging 8 h
D5		None	None	Natural aging 24 h
D6		None	None	Natural aging 48 h

2.3. Mechanical Properties and Microstructure Test

Samples for optical observation and mechanical property testing were cut from a seamless tube, as shown in Figure 2a. The optical samples were firstly ground with 200-, 400-, 800-, 1500- and 2000-grit sandpapers, then mechanically polished on a gold velvet disk sprayed with 1 μm diamond powder at 2000 rpm for 5 min, and finally chemically etched with Keller's reagent. The chemical composition of the Keller's reagent was an aqueous solution with 2.5%HNO_3, 1.5%HCl, and 1%HF; the etching time was 25 s. The pre-stretched test specimens were prepared by processing round bars with a diameter of 18 mm and a length of 300 mm, as in Figure 2b. Each side of the round bar has a clamping section 50 mm in length. During the pre-stretching process, no plastic deformation occurs in the clamping sections. Therefore, when sampling for mechanical property testing, the clamping sections should be avoided. The standard round tensile specimen processed with an M16 thread and a length of 100 mm is shown in Figure 2c. Under each heat treatment condition, four round tensile specimens are processed and tested to avoid the randomness of test data. The average mechanical properties are calculated based on the final statistics, and a bar chart of mechanical properties is plotted with standard deviation as the error bars. The tensile properties were measured using an Instron 5569 testing machine (Instron, Norwood, MA, USA). The test error of the equipment is less than 1%. The wire electrical discharge

machining (WEDM) marks on the surface are removed through mechanical processing. The SEM/EBSD observation was conducted on a Zeiss Supra55 scanning electron microscope (Zeiss, Oberkochen, Germany). The TEM observation was carried out by using a Talos F200X transmission electron microscope (Thermo Fisher Scientific, Waltham, MA, USA).

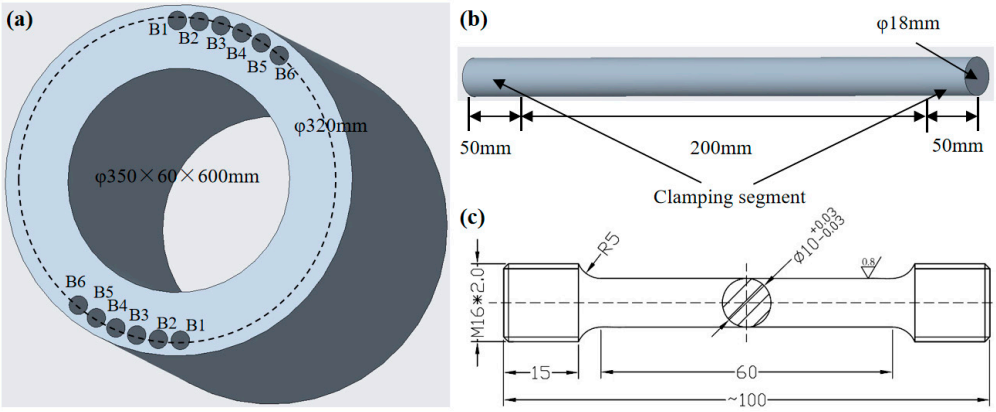


Figure 2. (**a**) Schematic diagram of sampling locations, (**b**) dimensional diagram of pre-stretch bar, (**c**) dimensional diagram of tensile test specimen.

3. Results and Discussion

3.1. Pre-Stretching Treatment

The B2 to B5 groups were all subjected to solution treatment followed by pre-stretching, with the interval between solution quenching and pre-stretching controlled within half an hour. The cumulative plastic deformation of pre-stretching was 2%. The stress–strain curve for pre-stretching is shown in Figure 3.

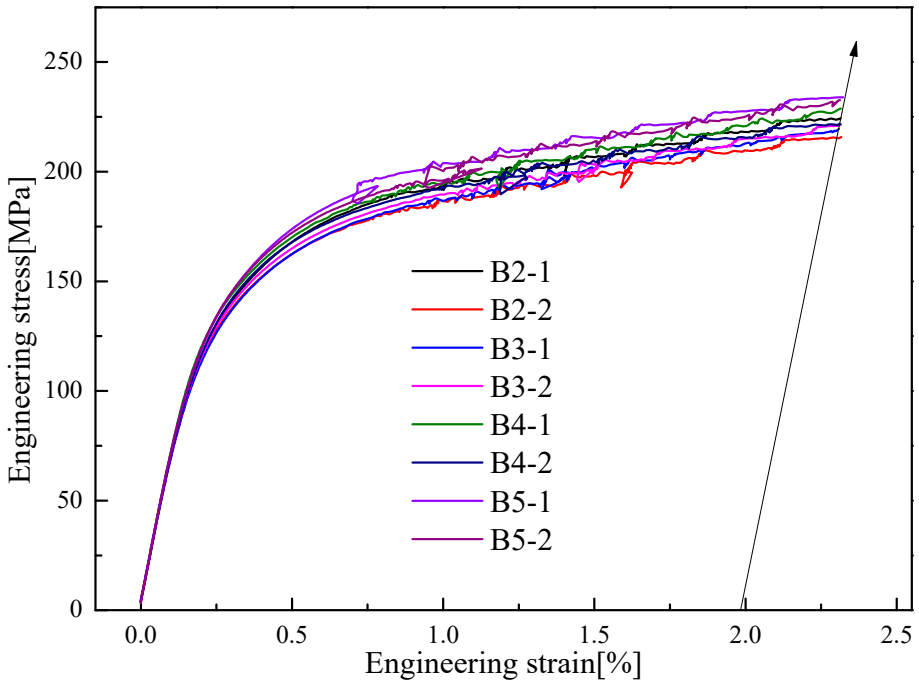


Figure 3. The stress–strain curve of pre-stretched samples in group B.

3.2. Mechanical Properties

The tensile mechanical properties of Group A and Group B are shown in Figure 4. Comparing the mechanical properties of Group A1 and Group B1, Group A1 exhibits a

yield strength ranging from 478 to 481 MPa and a tensile strength ranging from 590 to 592 MPa, both of which are over 100 MPa higher than those of Group B1. However, the elongation of Group A1, ranging from 14.5% to 16.0%, is 0.5% to 2% lower than that of Group B1. Comparing the mechanical properties of Group A2 and Group B6, Group A2 has a yield strength of 497~498 MPa, a tensile strength of 540~541 MPa, and an elongation of 15%; Group B6 has a yield strength of 437~438 MPa, a tensile strength of 484~486 MPa, and an elongation of 13.5~14.5%. The yield strength, tensile strength, and elongation of Group A2 are all higher than those of Group B6. Based on the comprehensive comparison of the mechanical properties of Groups A1, A2, B1, and B6, it is evident that the overall mechanical properties of the materials in Group A with an extrusion ratio of 12 are superior to those in Group B.

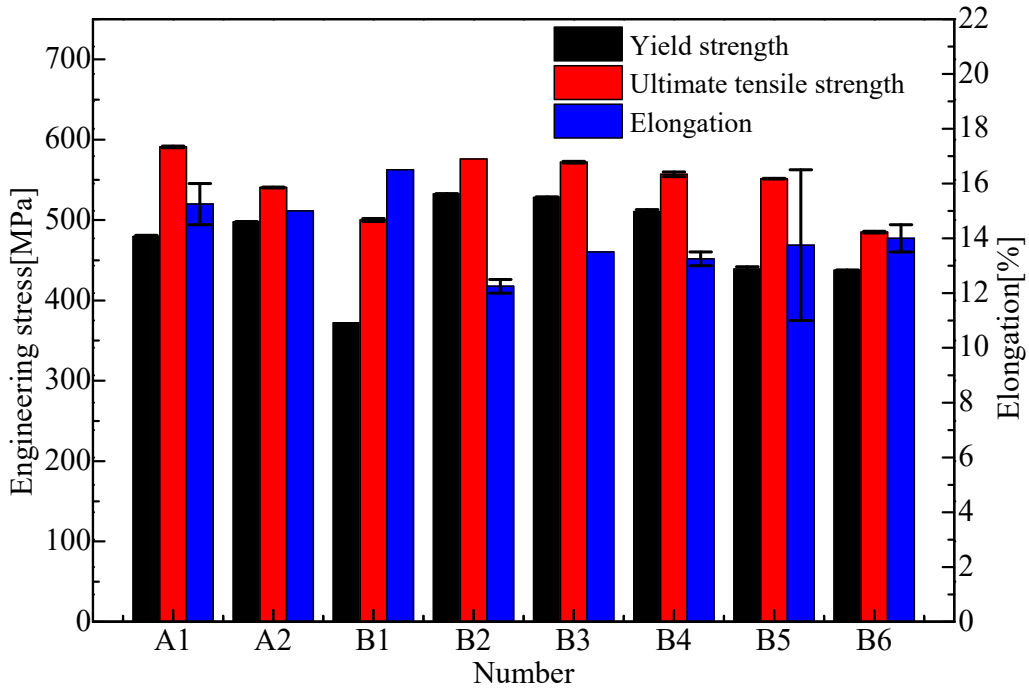


Figure 4. The mechanical property results of samples from Group A and Group B.

Figure 5 shows the low-magnification and metallographic images of the samples from Groups A and B. The microstructure of Group A consists of an α-Al matrix with compound phases, while the microstructure of Group B comprises an α-Al matrix, compound phases, and dispersed particle phases. When comparing the microstructures of Groups A and B, Group A exhibits large elongated grains and numerous small equiaxed grains, with the particle phases primarily distributed at the grain boundaries. In contrast, Group B predominantly features coarse elongated deformed grains, with fewer equiaxed grains than in Group A's samples and larger equiaxed grain sizes. The dispersed particle phases are not only located at the grain boundaries but also abundantly present within the grains. Based on the comprehensive comparison of mechanical properties and microstructures, Group A, with a larger extrusion ratio, achieves a dynamic recrystallized microstructure characterized by the coexistence of large elongated grains and small fine equiaxed grains. Additionally, the distribution of particle phases in Group A is more reasonably controlled, resulting in better mechanical properties compared to Group B.

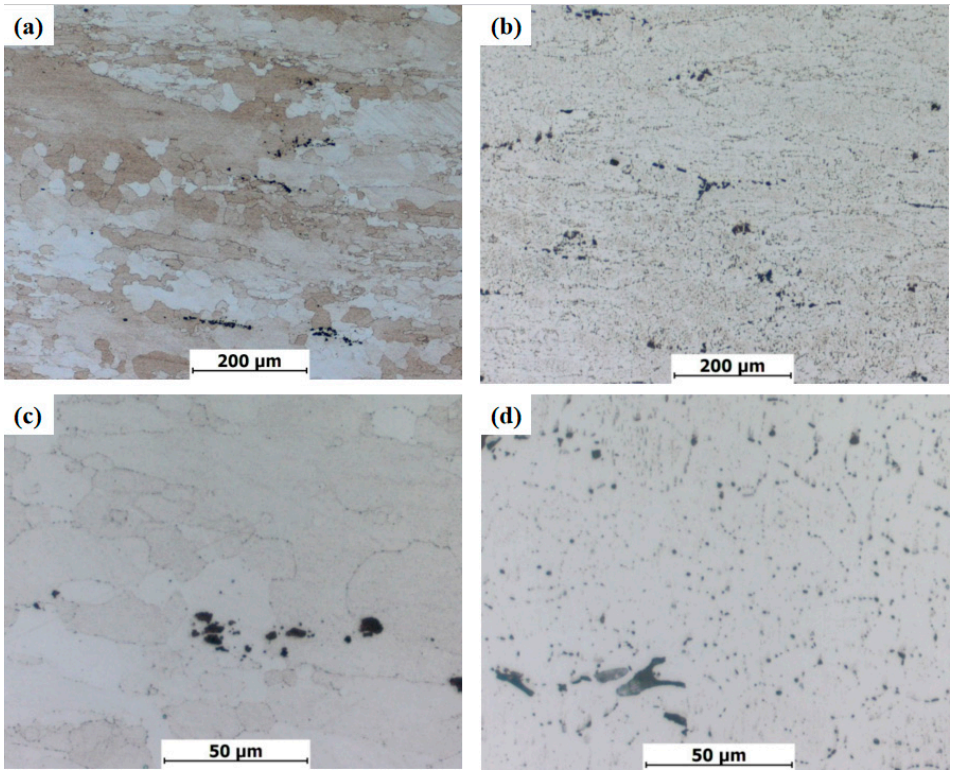


Figure 5. Microstructural properties of (**a**) group A 50×, (**b**) group B 50×, (**c**) group A 200×, (**d**) group B 200×.

The tensile properties of Group C samples under different heat treatment conditions are shown in Figure 6. By comparing the results of samples B2–B4, it is evident that the interval between pre-stretching and aging significantly affects the properties of Er-containing 7075 aluminum alloy: the shorter the interval between pre-stretching and aging (B2 with a 24 h interval), the higher the yield strength and tensile strength of the Er-containing 7075 aluminum alloy; appropriately extending the interval (B3 with a 15-day interval) can trade off a small amount of tensile strength for a certain degree of elongation at break; further extending the interval (B4 with a 30-day interval) results in a noticeable decrease in tensile strength, with almost no change in elongation at break, thus deteriorating the mechanical properties of the alloy. When comparing the samples C1–C8 without pre-stretching, the tensile strength of er-containing 7075 aluminum alloy first increases to a peak (C3) and then decreases, reaching its peak during aging (120 °C × 6 h + 163 °C × 3 h). Among them, the dual-stage aging system of sample C6 is close to the aging system of samples B2–B4. The tensile strength of C6 is lower than that of B2 and B3, but higher than that of B4, indicating that when the interval between pre-stretching and aging is less than 15 days, the pre-stretching process can significantly enhance the tensile strength of Er-containing 7075 aluminum alloy; however, when the interval exceeds 30 days, the pre-stretching process does not strengthen the tensile strength of Er-containing 7075 aluminum alloy.

Fracture toughness tests were performed on the Group C samples, and the test results are shown in Table 3. It can be seen that the KIC value of the alloy decreases with the increase in aging time. This is due to the increase in the volume fraction of precipitates with the increase in aging time, which hinders the movement of dislocations and improves the tensile strength, but the brittleness increases significantly.

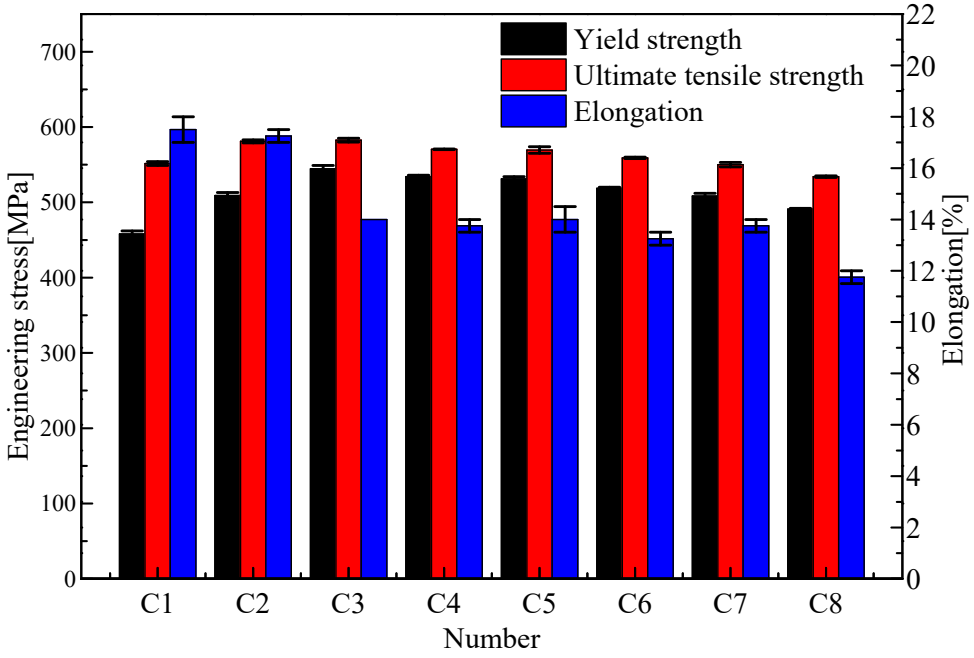


Figure 6. The mechanical property results of samples from Group C.

Table 3. KIC test results of Er-containing 7075 aluminum alloy.

Number	P_Q/kN	P_{max}/kN	P_{max}/P_Q	K_Q/MPa·m$^{1/2}$	K_{IC}/MPa·m$^{1/2}$
C2	5.87	5.87	1.00	31.89	31.89
C4	5.04	5.04	1.00	28.86	28.86
C6	4.73	4.73	1.00	26.76	26.76

Tensile performance tests were conducted on samples that underwent natural aging for 0.5 h, 2 h, 4 h, 8 h, 24 h, and 48 h after solution treatment, with the results presented in Figure 7. As the natural aging time increased, both the yield strength and tensile strength gradually rose, while the elongation first increased and then remained stable. After 48 h of natural aging, the yield strength of the alloy was only 300 MPa, and the tensile strength was just 465 MPa. With the extension of natural aging time, the elongation of 7075 aluminum alloy increases slightly in the early stage, and then decreases to a certain extent and becomes stable. The increase in elongation in the initial stage of natural aging is the result of the fine coherent GP zone optimizing the deformation uniformity, restraining the local strain concentration and weakening the grain boundary. As aging proceeds, the formation of incoherent η′ phase disrupts this mechanism, leading to a plastic fallback and eventual stabilization.

3.3. Microstructure and Fracture Behavior

Figure 8 shows the EBSD-IPF images of Er-containing 7075 alloy on the ED-TD plane. The Electron Backscattered Diffraction (EBSD) analysis of the hot-extruded aluminum alloy microstructure reveals a fascinating array of structural characteristics that are instrumental in understanding its mechanical properties and performance. The hot extrusion process subjects the alloy to significant deformation under high temperatures, leading to a complex microstructural evolution. Here, we delve into the distinct features observed through EBSD testing, which provide deep insights into the grain structure, orientation, and potential sites of mechanical weakness.

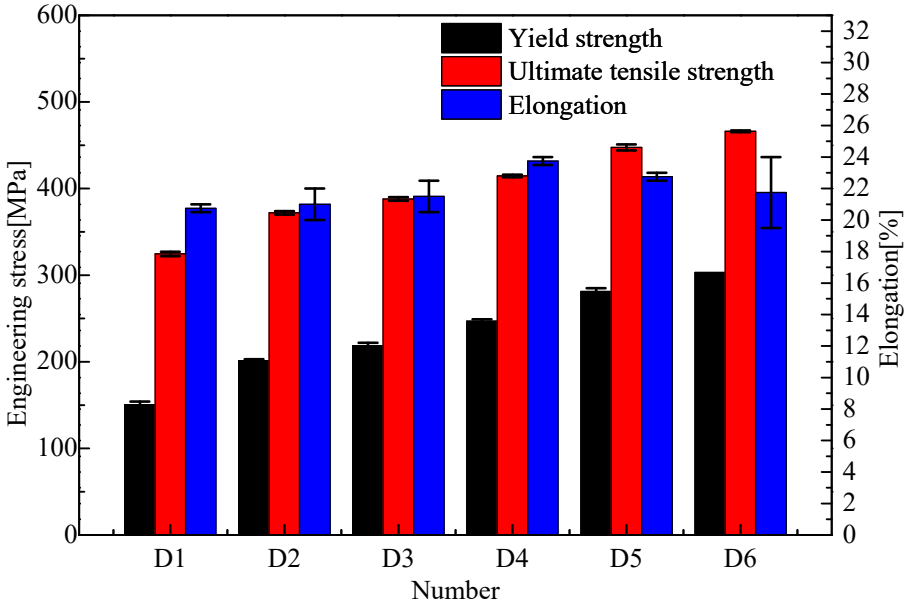


Figure 7. The mechanical property results of samples from Group D.

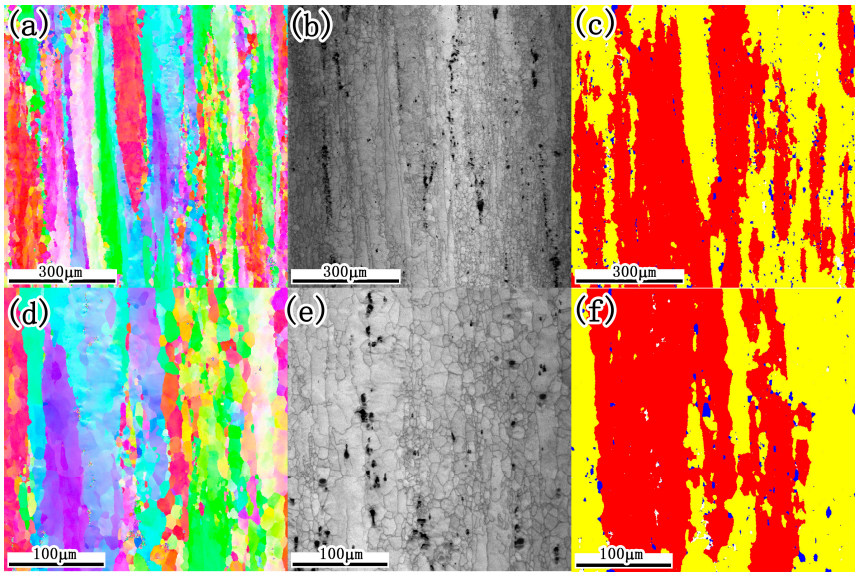


Figure 8. EBSD images of Er-containing 7075 Al alloy on ED-TD plane: (**a**) IPF image of B2-200×, (**b**) IQ image of B2-200×, (**c**) GOS image of B2-200×, (**d**) IPF image of B2-500×, (**e**) IQ image of B2-500×, (**f**) GOS image of B2-500×.

The primary observation from the EBSD maps is the presence of a dynamically recrystallized microstructure. During hot extrusion, the high temperatures and shear forces facilitate the formation of new grains through the process of recrystallization. These grains tend to be smaller and more equiaxed compared to the initial coarse grains, contributing to an overall refinement of the microstructure. The EBSD analysis clearly shows these recrystallized grains, which are evenly distributed throughout the material, indicating a good degree of homogeneity in the microstructure.

Furthermore, the EBSD data reveals the orientation of these grains. In hot-extruded alloys, grains often exhibit a preferred orientation due to the directional nature of the extrusion process. This preferential alignment can be visualized through misorientation maps, which show the angle between adjacent grains. The presence of low-angle grain boundaries (LAGBs) and high-angle grain boundaries (HAGBs) provides information about the degree of grain fragmentation and recrystallization. In a well-recrystallized

microstructure, a higher proportion of HAGBs is typically observed, indicating a more random grain orientation and thus improved mechanical properties.

In addition, there was a phenomenon of texture in the hot-extrusion structure. The micro-texture of the corresponding region can be characterized by analyzing the EBSD results. Figure 9 shows the pole figure of Er-containing 7075 alloy at hot-extrusion stage. The pole figures shows the distribution of texture in {001}, {111} and {110}. There was an obvious texture phenomenon in the hot extrusion structure, and the intensity of texture was the highest at {111}, and the peak intensity of texture reached 7.638.

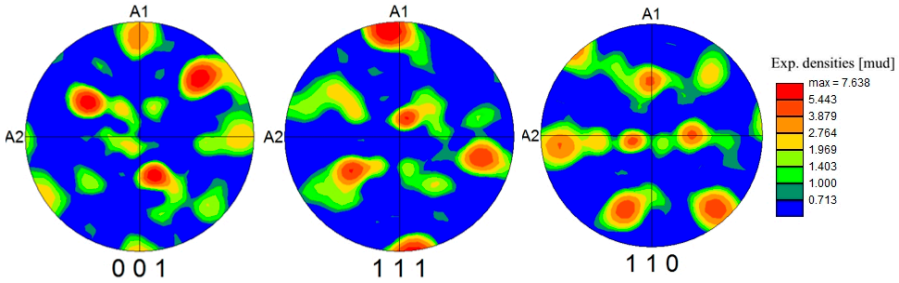


Figure 9. Figure shows {001}, {111}, and {110} pole figures of er-containing 7075 Al alloy.

Figure 10 shows the transmission electron microscope bright-field image of Er-containing 7075 aluminum alloy under peak aging. There were uniformly distributed submicron FeMnSi phases in the alloy crystals. The sample was taken from the tensile sample of peak aging, and the alloy had undergone plastic deformation under tensile action. In the process of tensile deformation, the sub-micron FeMnSi met as the particle of the pinning dislocation, preventing further slip of the dislocation (see Figure 10b), and playing a certain role of second phase strengthening. The sub-micron FeMnSi phase (see Figure 10d) distribution was uniform and the size was small, which played a good role in strengthening the alloy. Er modified aluminum alloy precipitation via nanoscale Al_3Er nucleation, solute diffusion control, and co-precipitation design, quantified by models like ClaNG (thermodynamics) and vacancy-enhanced JMAK (kinetics). According to the JMAK mechanism, the volume fraction of Al_3Er increases with the increase in aging time, and gradually coarsens and grows up.

The η-$MgZn_2$ phase (see in Figure 10c) aging precipitation sequence of 7075 aluminum alloy can be expressed as follows: α-Al (susaturated solid solution)→{(Mg, Zn) atomic clusters}→{G-P regions}→{coherent η″ transition precipitated phase}→{semi-coherent η′ transition precipitated phase}→non-coherent η-$MgZn_2$ equilibrium phase}.

Figure 11 shows the morphology of the tensile fracture of the Er-containing 7075 aluminum alloy. At a lower magnification, the macro morphology of the fracture shows a certain river pattern morphology (see in Figure 11a,b), indicating that the fracture is more brittle than normal, which is consistent with the lower fracture elongation. Further enlarging the fracture morphology (see in Figure 11c), it can be observed that there is a very small dimple morphology on the fracture, and a relatively obvious tearing edge structure can be observed, which indicates that the part has a certain fracture toughness. When the magnification is further increased (see in Figure 11d), it can be seen that some of the second phase positions are very flat fracture morphology, while the Al matrix is dominated by dimple morphology. It shows that the fracture mechanism of the parts is a hybrid fracture form combining ductile fracture and brittle fracture. The energy spectrum analysis is carried out at the crack source in Figure 11d, and the results are shown in Figure 11e. The crack source of fracture in Er-containing 7075 aluminum alloy is the segregated second phases containing Cu and Er in the alloy, with the size of these alloy phases being around 10 micrometers.

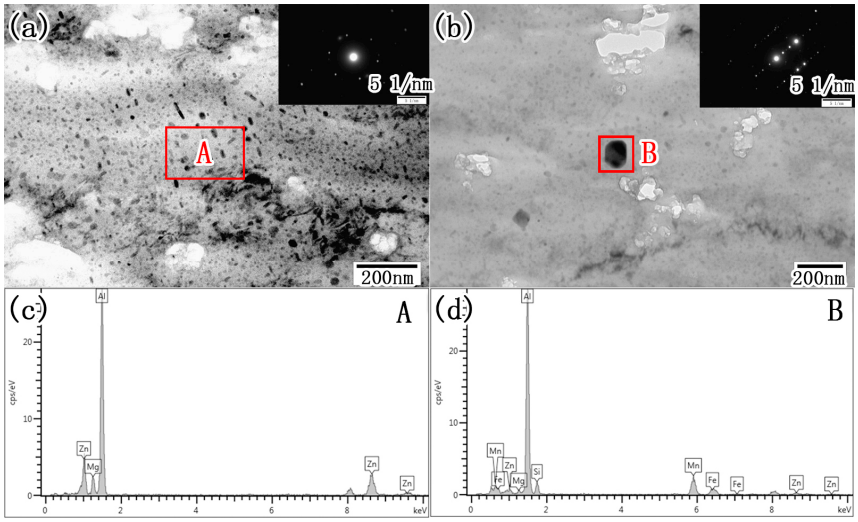
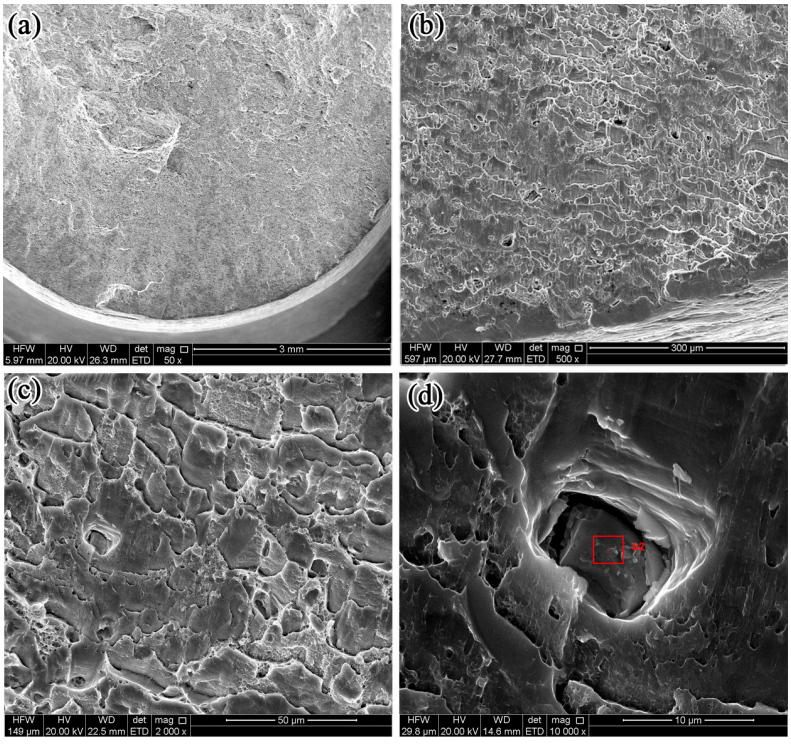
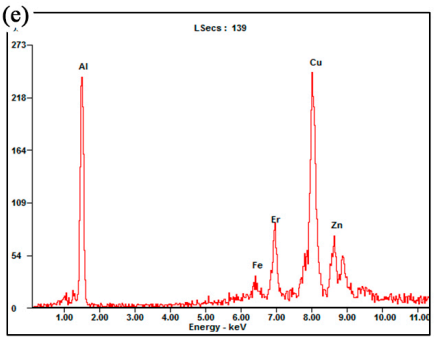


Figure 10. TEM bright-field image of Er-containing 7075 aluminum alloy: (**a**) tilting to clear angle of dislocation; (**b**) tilting to a dislocation is almost invisible; (**c**) EDS results of region A in (**a**); (**d**) EDS results of region B in (**b**).





Element	*Wt %*	*At %*
MgK	00.53	01.31
AlK	14.39	32.19
FeK	02.33	02.52
ErL	24.18	08.73
CuK	42.85	40.72
ZnK	15.73	14.53

Figure 11. Fracture surfaces of the B2 specimens: (**a**) 50×, (**b**) 500×, (**c**) 2000×, (**d**) 10,000×, (**e**) energy-dispersive spectroscopy analysis result of the crack-initiation point.

4. Conclusions

In this paper, the microstructure and mechanical properties of different heat treatment parameters of Er-containing 7075 aluminum alloy were studied, and the effects of the pre-stretch and the interval time between pre-deformation and artificial aging on mechanical properties of Er-containing 7075 aluminum alloy were systematically studied. The optimum heat treatment parameters for Er-containing 7075 wrought aluminum alloy were obtained by testing the mechanical properties. The research results have significant engineering significance for the optimization of the heat treatment process of Er-containing 7075 aluminum alloy. The main conclusions are as follows:

(1) Increasing the extrusion ratio during the hot extrusion process can significantly enhance the mechanical properties of Er-containing 7075 aluminum alloy.
(2) Pre-stretching can provide nucleation sites for the precipitation of reinforcing phases, accelerate the aging strengthening process, and shorten the peak aging time.
(3) The crack source of fracture in Er-containing 7075 aluminum alloy is the segregated second phases containing Cu and Er in the alloy, with the size of these alloy phases being around 10 micrometers.
(4) The optimal heat treatment process for the Er-7075 alloy is 470 °C × 1 h + 500 °C × 2 h, with water quenching, a pre-stretching deformation of 2%, and double-stage aging at 110 °C × 5 h + 150 °C × 12 h.

Author Contributions: Conceptualization, Y.L., Z.L. and D.W.; methodology, Y.L., G.L. and D.W.; validation, Z.L., W.L., L.C. and Y.W.; formal analysis, Y.L., W.L. and Y.Y.; investigation, Y.L. and J.R.; resources, G.L. and D.W.; data curation, Y.L., D.W. and Y.Y.; visualization, J.R.; supervision, Z.L. and L.C.; project administration, Z.L. and Y.W. All authors have read and agreed to the published version of the manuscript.

Funding: This research received no external funding.

Data Availability Statement: The original contributions presented in this study are included in the article. Further inquiries can be directed to the corresponding authors.

Conflicts of Interest: Authors Yingze Liu, Zhiqian Liao, Desheng Wang, Guoyuan Liu, Jiangyi Ren, Wenfu Li, Yunao Yang, Lingjie Chen and Yue Wang were employed by Luoyang Ship Material Research Institute.

References

1. Huang, L.; He, L.; Chen, S.; Chen, K.; Li, J.; Li, S.; Liu, W. Effects of non-isothermal aging on microstructure, mechanical properties and corrosion resistance of 2A14 aluminum alloy. *J. Alloys Compd.* **2020**, *842*, 155542. [CrossRef]
2. Shi, C.; Wu, Y.; Mao, D.; Fan, G. Effect of Ultrasonic Bending Vibration Introduced by the L-shaped Ultrasonic Rod on Solidification Structure and Segregation of Large 2A14 Ingots. *Materials* **2020**, *13*, 807. [CrossRef] [PubMed]
3. Yu, W.; Zhan, L.; Xu, Y.; Chen, K.; Yang, Y.; Xu, L.; Peng, N.; Ma, B.; Liu, C.; Chen, Z. Temperature-dependent creep aging behavior of 2A14 aluminum alloy. *J. Mater. Res. Technol.* **2022**, *19*, 1343–1354. [CrossRef]
4. Wang, B.; Yi, Y.; He, H.; Huang, S. Effects of deformation temperature on second-phase particles and mechanical properties of multidirectionally-forged 2A14 aluminum alloy. *J. Alloys Compd.* **2021**, *871*, 159459. [CrossRef]
5. Lan, J.; Shen, X.; Liu, J.; Hua, L. Strengthening mechanisms of 2A14 aluminum alloy with cold deformation prior to artificial aging. *Mater. Sci. Eng. A* **2019**, *745*, 517–535. [CrossRef]
6. Zinong, T.; Bing, Z.; Jun, J.; Zhiqiang, L.; Jianguo, L. A study on the hot roll bonding of aluminum alloys. *Procedia Manuf.* **2020**, *50*, 56–62. [CrossRef]
7. Qian, X.; Li, X.; Li, Y.; Xu, G.; Wang, Z. Microstructure evolution during homogenization and hot workability of 7055 aluminum alloy produced by twin-roll casting. *J. Mater. Res. Technol.* **2021**, *13*, 2536–2550. [CrossRef]
8. Zhu, Z.; Hu, Z.; Seet, H.L.; Liu, T.; Liao, W.; Ramamurty, U.; Ling Nai, S.M. Recent progress on the additive manufacturing of aluminum alloys and aluminum matrix composites: Microstructure, properties, and applications. *Int. J. Mach. Tools Manuf.* **2023**, *190*, 104047. [CrossRef]

9. Honarmand, M.; Salehi, M.; Shabestari, S.G.; Saghafian, H. Impact strength and structural refinement of A380 aluminum alloy produced through gas-induced semi-solid process and Sr addition. *Trans. Nonferrous Met. Soc. China* **2022**, *32*, 1405–1415. [CrossRef]
10. Li, G.; Qu, W.; Luo, M.; Cheng, L.; Guo, C.; Li, X.; Xu, Z.; Hu, X.; Li, D.; Lu, H.; et al. Semi-solid processing of aluminum and magnesium alloys: Status, opportunity, and challenge in China. *Trans. Nonferrous Met. Soc. China* **2021**, *31*, 3255–3280. [CrossRef]
11. Qi, M.; Kang, Y.; Li, J.; Wulabieke, Z.; Xu, Y.; Li, Y.; Liu, A.; Chen, J. Microstructures refinement and mechanical properties enhancement of aluminum and magnesium alloys by combining distributary-confluence channel process for semisolid slurry preparation with high pressure die-casting. *J. Mater. Process. Technol.* **2020**, *285*, 116800. [CrossRef]
12. Liu, F.; Dong, P.; Khan, A.S.; Zhang, Y.; Cheng, R.; Taub, A.; Ma, Z. 3D printing of fine-grained aluminum alloys through extrusion-based additive manufacturing: Microstructure and property characterization. *J. Mater. Sci. Technol.* **2023**, *139*, 126–136. [CrossRef]
13. Tang, S.; Yang, Y.; Yang, L.; Fan, Z. A green extrusion-based 3D printing of hierarchically porous aluminum. *Powder Technol.* **2022**, *399*, 117198. [CrossRef]
14. Faster 3D printing of aluminum. *Met. Powder Rep.* **2021**, *76*, 215. [CrossRef]
15. Zhang, P.; Liu, J.; Gao, Y.; Liu, Z.; Mai, Q. Effect of heat treatment process on the micro machinability of 7075 aluminum alloy. *Vacuum* **2023**, *207*, 111574. [CrossRef]
16. El Garchani, F.E.; Lgaz, H.; Kaya, S.; Lee, H.-S.; Ibrahim, S.M.; Chafiq, M.; Ko, Y.G.; Kabiri, M.R. Effects of Heat Treatment on the Corrosion Behavior and Mechanical Properties of Aluminum Alloy 2024. *J. Mater. Res. Technol.* **2023**, *25*, 1355–1363. [CrossRef]
17. Chen, Q.; Zhao, W.; Jiang, J.; Huang, M.; Li, M.; Wang, Y.; Ding, C.; Zou, D. Effect of T6 heat treatment on microstructure and mechanical properties of large-weight aluminum alloy flywheel housing parts formed by local-loading squeeze casting. *J. Mater. Res. Technol.* **2023**, *24*, 1612–1625. [CrossRef]
18. Xiao, A.; Lin, Y.; Huang, C.; Cui, X.; Yan, Z.; Du, Z. Effect of electromagnetic forming–heat treatment process on mechanical and corrosion properties of 2024 aluminum alloy. *J. Mater. Res. Technol.* **2023**, *23*, 1027–1038. [CrossRef]
19. Singh, S.P.; George, D.T.; Xavier, A.A.J.; Raja, G.A. Effect of heat treatment on the hardness behaviour of the aluminium 6061 alloy. *Mater. Today Proc.* **2023**, *in press*. [CrossRef]
20. Chen, Q.; Chen, G.; Ji, X.; Han, F.; Zhao, Z.; Wan, J.; Xiao, X. Compound forming of 7075 aluminum alloy based on functional integration of plastic deformation and thixoformation. *J. Mater. Process. Technol.* **2017**, *246*, 167–175. [CrossRef]
21. Lin, B.; Fan, T.; Li, H.; Zhao, Y.; Zhang, W.; Liu, K. Microstructure and high temperature tensile properties of Al–Si–Cu–Mn–Fe alloys prepared by semi-solid thixoforming. *Trans. Nonferrous Met. Soc. China* **2021**, *31*, 2232–2249. [CrossRef]
22. Li, G.F.; Zhang, X.M.; Zhu, H.F. Effect of minor er and y additions to Al-Zn-Mg-Cu-Zr alloy on homogenizing behavior. *J. Aeronaut. Mater.* **2010**, *30*, 1–6.
23. Wu, H.; Wen, S.P.; Lu, J.T.; Mi, Z.P.; Zeng, X.L.; Huang, H. Microstructural evolution of new type Al–Zn–Mg–Cu alloy with Er and Zr additions during homogenization. *Trans. Nonferrous Met. Soc. China* **2017**, *27*, 1476–1482. [CrossRef]
24. Shuai, Y.; Lina, J.; Hu, Z. Effects of Er on the Microstructure and Eutectic Phase Morphology of Directionally Solidified Al-Zn-Mg-Cu-Zr Alloys. *Rare Met. Mater. Eng.* **2021**, *50*, 3477–3484. [CrossRef]
25. Chen, G.; Chen, Q.; Qin, J.; Du, Z. Effect of compound loading on microstructures and mechanical properties of 7075 aluminum alloy after severe thixoformation. *J. Mater. Process. Technol.* **2016**, *229*, 467–474. [CrossRef]
26. Zhang, Y.; Yi, Y.; Huang, S.; Dong, F.; Wang, H. Investigation of the quenching sensitivity of forged 2A14 aluminum alloy by time-temperature-tensile properties diagrams. *J. Alloys Compd.* **2017**, *728*, 1239–1247. [CrossRef]
27. Menargues, S.; Martín, E.; Baile, M.T.; Picas, J.A. New short T6 heat treatments for aluminium silicon alloys obtained by semisolid forming. *Mater. Sci. Eng. A* **2015**, *621*, 236–242. [CrossRef]
28. Liu, Y.; Chen, X.; Gao, M.; Guan, R. Enhanced strength-ductility synergy in a rheo-diecasting semi-solid aluminum alloy. *Mater. Lett.* **2021**, *305*, 130756. [CrossRef]
29. Ragheb, Z.D.; Shabestari, S.G.; Najafi, Y. Effect of strain-induced melt activation process and thixoforming on microstructure and mechanical properties of 319 aluminum alloy. *J. Alloys Compd.* **2023**, *954*, 170152. [CrossRef]

Disclaimer/Publisher's Note: The statements, opinions and data contained in all publications are solely those of the individual author(s) and contributor(s) and not of MDPI and/or the editor(s). MDPI and/or the editor(s) disclaim responsibility for any injury to people or property resulting from any ideas, methods, instructions or products referred to in the content.